The influence of spin orbit interaction on phonons and superconductivity in the noncentrosymmetric superconductors LaPt$_3$Si and LaPtSi$_3$

H. Y. Uzunok[a,b], H. M. Tütüncü[a,b] G. P. Srivastava[c] and A. Başoğlu[a,b]

[a] *Sakarya Üniversitesi, Fen-Edebiyat Fakültesi, Fizik Bölümü, 54187, Adapazarı, Turkey*

[b] *Sakarya Üniversitesi, BIMAYAM, Biyomedikal, Manyetik ve Yarıiletken Malzemeler Araştırma Merkezi, 54187, Sakarya , Turkey*

[c] *School of Physics, University of Exeter, Stocker Road, Exeter EX4 4QL, UK*

Abstract

We have performed *ab initio* study of structural, electronic, vibrational and electron-phonon interaction properties of LaPt$_3$Si and LaPtSi$_3$ by employing the density functional theory, a linear-response formalism, and the plane-wave pseudopotential method. The electronic structure, phonon dispersion relations and the Eliashberg spectral function for these materials have been examined with and without the inclusion of spin-orbit interaction (SOI). Our electron-phonon interaction results reveal that the influence of spin-orbit interaction on phonons and superconductivity in these noncentrosymmetric superconductors is very small. Thus, we can conclude that a mixing of the spin-singlet and the spin-triplet components in these superconductors is weak and the spin-singlet Cooper pairs dominate. By integrating the Eliashberg spectral function $\alpha^2 F(\omega)$, the average electron-phonon coupling parameter λ is obtained to be 0.470 for LaPt$_3$Si and 0.488 for LaPtSi$_3$, indicating these to be weak-coupling BCS superconductors. Using an acceptable value of μ^* = 0.13 for the effective Coulomb repulsion parameter, the superconducting critical temperature T_c is calculated to be 0.67 K for LaPt$_3$Si and 1.39 K for LaPtSi$_3$, in good accordance with experimental values of 0.65 K and 1.52 K, respectively.

Key words: A. intermetallics; B.density functional theory,electronic structure, superconducting properties; E. abinitio calculations, physical properties

[1] Corresponding Author: H. M. Tütüncü Tel: +90 264 295 60 72 Fax: +90 264 295 59 50 e-Mail: tutuncu@sakarya.edu.tr

Noncentrosymmetric (NCS) superconductors have been known for decades but have become an outstanding research topic recently following the discovery of superconductivity in $CePt_3Si$ [1]. The superconducting order parameters in NCS superconductors cannot be categorized in terms of parity, and the coexistence of both spin-singlet and spin-triplet states is permitted [2–6]. Two types of NCS superconductors have been noted: strongly correlated systems such as $CePt_3Si$ [1] and UIr [7], and weakly correlated systems such as Li_2Pt_3B and Y_2C_3 [8,9]. The superconducting properties of heavy-fermion NCS superconductors are strongly affected by electron correlation effects, and the weakly correlated NCS superconductors provide a fertile ground for studying mixing of the singlet-triplet pairing derived from the break down of inversion symmetry and a strong Rashba-type asymmetric spin-orbit-coupling (ASOC) interaction. Despite the anticipation of mixed parity pairing in NCS superconductors, single-gap BCS-like superconductivity is clearly found in many NCS superconductors. For instance, $LaPt_3Si$ (with superconducting transition temperature $T_c = 0.65$ K), which is isostructural with $CePt_3Si$, displays no sign of magnetic order or strong electronic correlation. Thus, $LaPt_3Si$ is expected to be an ideal system for studying the effect of the lack of inversion symmetry on the superconducting state [1,10–14]. In addition, similar to $LaPt_3Si$, NCS superconductors such as $BaPtSi_3$ [15], $LaRhSi_3$ [16], $CaPtSi_3$ [17,18], $CaIrSi_3$ [17,18], $LaPtSi_3$ [19] and $LaPdSi_3$ [19] also do not exhibit strong electronic correlations, and exhibit superconductivity with the BCS characteristics at ambient pressure. Recently, Krannich and co-workers [20] have measured the dispersion of transverse acoustic and low energy optical phonon branches for $CePt_3Si$ along the [110] direction using inelastic neutron scattering . In these branches they have found deviations from their *ab initio* lattice dynamical calculations, which overall gives good explanation of the phonon dispersion in $CePt_3Si$. Thus, they emphasize that the lattice dynamics of $CePt_3Si$ is conventional and that the observed deviations between their experimental and theoretical calculations are not linked to effects of ASOC. These authors have also mentioned that a strong Rashba-type ASOC plays less a role in noncentrosymmetric superconductors than widely believed [20].

The discovery of superconductivity in NCS materials has motivated theoretical physicists to study their structural, electronic, vibrational and superconducting properties. Bauer and co-workers [15] have studied electronic, phononic and superconducting properties of $BaPtSi_3$ by using the density functional theory (DFT) within the local density approximation (LDA). This theoretical work [15] has mentioned that the non-inversion symmetry plays only a minor role for the superconducting properties of $BaPtSi_3$ due to rather small spin-orbit splitting at the Fermi energy level. The electronic structures of $CaPtSi_3$ and $CaIrSi_3$ have been calculated by means of the full-potential linearised augmented plane wave (FLAPW) [21]. This theoretical work [21] reveals that the electronic structures of these superconductors display similarities to the corresponding structure of $BaPtSi_3$ [15]. Terashima and co-workers [22] have performed angle-resolved de Hass-van Alphen (dHvA) measurements and FLAPW band-structure calculations for $LaRhSi_3$. They have indicated that the dHvA frequency branches observed in this superconductor can quantitatively be described by the calculated Fermi surface, which is composed of three pairs of inversion-asymmetry-split sheets. The electronic properties of $LaPdSi_3$ have

2

been investigated by using the full-potential local-orbital method (FPLO) within the density functional theory [23]. This theoretical work reveals that the influence of spin-orbit coupling in this NCS superconductor, particularly in small energy range around the Fermi level, is rather low. Recently, the electronic structure of $LaPt_3Si$ has been calculated by using the DFT within the LDA [20]. Very recently, Uzunok and co-workers [24] have carried out an *ab initio* study of the electronic, vibrational and electron-phonon interaction properties of $CaIrSi_3$ by employing the DFT, a linear response formalism, and the plane-wave pseudopotential method. This theoretical work reveals that the influence of spin-orbit interaction (SOI) on the average electron-phonon coupling parameter is very small. Thus, Uzunok and co-workers [24] conclude that a mixing of the spin-singlet and the spin-triplet components in the superconducting condensate is weak and the spin-singlet Cooper pairs dominate.

In spite of some theoretical progress in examining the electronic properties of $LaPt_3Si$, no experimental or theoretical works have been performed to investigate the electronic properties of $LaPtSi_3$. Furthermore, the electron-phonon interaction properties of these materials have not yet been investigated. It is important to examine the spectral distribution function of the electron-phonon interaction as a number of important physical properties of solids are governed by it, such as the electrical and thermal resistivities, superconductivity, softening of phonon modes, renormalization of the low-temperature electronic component of the heat capacity, and a number of other physical phenomena. For this reason, this work is aimed at making *ab initio* calculations of the structural and electronic properties of $LaPt_3Si$ and $LaPtSi_3$ by using a generalized gradient approximation (GGA) of the DFT with and without the inclusion of spin-orbit interaction (SOI) [25]. We have further performed *ab initio* linear response calculations [25] of phonon dispersion relations and electron-phonon matrix elements in these NCS materials. A detailed comparison of the SOI and non-SOI electronic structures and the electron-phonon matrix elements is made. The phonon density of states and the electron-phonon matrix elements are used to determine the Eliashberg spectral function [26,27], from which the average electron-phonon coupling parameter can be determined. Using the average electron-phonon coupling parameter and the logarithmic average of phonon frequency, we finally compute the superconducting transition temperature.

1 Theory

All calculations have been made using the density functional theory with and without SOI. We have used the plane wave-pseudo-potential method as implemented in the QUANTUM-ESPRESSO simulation package. The atomic pseudopotentials generated using the projected-augmented wave [25] (PAW) are used to simulate interactions between valence electrons and ion cores, and the electron wave function is expanded in plane waves up to an energy cutoff of 60 eV for all calculations. The electron exchange–correlation energy is evaluated using the GGA of the Perdew–Burke–Ernzerhof (PBE) formalism [28]. Self-consistency in solutions to the Kohn-Sham equations [29] is achieved by considering special $\boldsymbol{k}$ points within the ir-

reducible Brillouin zone (IBZ). The energy calculations in the simple tetragonal IBZ have been made with a (8×8×8) $\boldsymbol{k}$-point mesh using the Monkhorst-Pack scheme [30] while a (24×24×24) Monkhorst-Pack $\boldsymbol{k}$-point grid has been utilized to describe the electronic properties of both materials.

Phonon calculations for both materials have been performed within the framework of the self-consistent density-functional perturbation theory[25] with and without SOI. Within this approach, second-order derivatives of the total energy are computed to determine the dynamical matrix. A static linear response of the valence electrons is considered in terms of the variation of the external potential corresponding to periodic displacements of the atoms in the unit cell. The screening of the electronic system in response to the displacement of the atoms has been taken into account in a self-consistent manner. We have used a (8×8×8) grid for sampling the irreducible segment of the Brillouin zone (BZ) in our phonon calculations for both materials. We find that the phonon frequencies for both studied materials are accurate to within 0.05 THz for the present choice of the kinetic energy cutoff and the special $\boldsymbol{k}$ points. In order to achieve phonon dispersion curves and density of states, we have computed 18 dynamical matrices for $LaPt_3Si$ and 13 dynamical matrices for $LaPtSi_3$ on a 4×4×4 grid in $\mathbf{q}$ space. Finally, these dynamical matrices have been Fourier transformed to procure the full phonon spectrum and density of states. The technique for the calculation of the electron-phonon interaction has been explained in detail in our previous study [32]. Fermi-surface sampling for the evaluation of the electron-phonon matrix elements has been made using 24×24×24 $\boldsymbol{k}$-mesh with a Gaussian width 0.02 Ry. The phonon density of states and the Eliashberg function have been also worked out using this $\boldsymbol{k}$-mesh.

2   Results

2.1   Structural and Electronic Properties

$LaPt_3Si$ crystallizes in a simple tetragonal $CePt_3B$-type crystal structure lacking inversion symmetry, with space group P4mm, and one formula unit per primitive unit cell. The five atoms inside a primitive unit cell can be grouped as four nonequivalent crystallographic sites: La, Pt1, Pt2, and Si according to the symmetry. The atomic positions are: La (1b) (1/2, 1/2, z_{La}), Pt1 (2c) (1/2, 0, z_{Pt1}), (0, 1/2, z_{Pt1}), Pt2 (1a) (0,0,0) and Si (1a) (0, 0, z_{Si}). As a consequence, this simple tetragonal structure is formed by two lattice parameters (a and c) and three internal parameters (z_{La}, z_{Pt1} and z_{Si}). The calculations have been performed to find total energy results, which are then fitted into Murnaghan equation of state to calculate bulk modulus (B). The calculated equilibrium lattice parameters (a and c), the equilibrium volume (V), the internal parameters (z_{La}, z_{Pt1} and z_{Si}), the Pt1-Si bond length (d_{Pt1-Si}), the Pt2-Si bond length (d_{Pt2-Si}) and the bulk modulus (B) are given in Tab. 1, together with previous experimental [1] and theoretical [20] results. The calculated lattice constants a and c vary from their experimental values [1] within 1.0% and

4

1.4%, respectively, while the calculated internal parameters are comparable with their LDA values [20]. However, to the best of our knowledge, experimental data is not available for bulk modulus. Fig. 1 displays the illustration of the tetragonal structure of LaPt$_3$Si, using the structural parameters from Tab. 1. Each Si atom coordinates with four basal Pt1 atoms and one apical Pt2 atom. The values of bond lengths are calculated to be 2.424 Å for the Pt1-Si bond and 2.326 Å for the Pt2-Si bond. These both values are shorter than the value of 2.47 Å determined from the summation of the atomic radii: 1.36 Å for Pt and 1.11 Å for Si. These results indicate strong covalent bonds between Pt and Si atoms.

LaPtSi$_3$ crystallizes in the body-centred tetragonal BaNiSn$_3$ of crystal structure with one formula unit per primitive unit cell is characterized with space group I4mm. The crystal structure, displayed in Fig. 2, has no mirror plane perpendicular to the z–axis. Each Pt atom is in five–fold coordination formed by four basal Si2 atoms and one apical Si1 atom. The atomic configuration in each unit cell is composed of one La atom at the (2a) (0, 0, 0) position, one Pt atom at (2a) (0.00, 0.00, z_{Pt}), one Si1 atoms at (2a) (0, 0, z_{Si1}) and two Si2 atoms at (4b) (0,1/2,z_{Si2}), (1/2, 0, z_{Si2}). Thus, this structure is characterized by two lattice parameters (a and c) and three internal parameters (z_{Pt}, z_{Si1} and z_{Si2}). The calculated equilibrium lattice parameters (a and c), the equilibrium volume (V), the internal parameters (z_{Pt}, z_{Si1} and z_{Si2}), the Pt-Si1 bond length (d_{Pt-Si1}), the Pt-Si2 bond length (d_{Pt2-Si}) and the bulk modulus (B) are given in Tab. 1, together with previous experimental results [19]. The variation of a and c from the recent experimental values [19] is 0.7% and 0.4%, respectively. However, to the best of our knowledge, experimental data does not exist for bulk modulus and the three internal parameters. The Pt-Si bond lengths are found to be 2.441 Å for Pt-Si1 and 2.360 Å for Pt-Si2. These values are shorter than the sum of the covalent radii of Pt and Si (2.47 Å) and thus suggest a strong covalent bonding between these atoms. Each Si1 atom is in four–fold coordination formed by four Si2 atoms with the interatomic distance of 2.544 Å. This distance is longer than the corresponding value of 2.352 Å in the diamond Si, thus indicating the presence of weaker Si-Si bond as compared to that in the diamond Si.

Fig. 3 displays the analysis of the band structure of LaPt$_3$Si with and without SOI. According to the calculated band structure, LaPt$_3$Si is a three-dimensional metal; some bands with large dispersion cross the Fermi level in spite of the apparent two dimensionality in its atomic structure. A comparison of the calculated band structures with and without SOI reveals that several degenerate bands are spin-orbit split but by different amounts. Of particular interest is to note that there is a clear, but small, splitting of bands in the window of ± 1.0 eV around the Fermi energy. The maximum band splitting in this energy window is 250 meV. However, the splitting of bands is very small close to the Fermi level. As a consequence, we can expect that a mixing of spin-singlet and spin-triplet components in the superconducting condensate is weak and spin-singlet Cooper pairs dominate.

The total and partial electronic density of states (DOS) with SOI for LaPt$_3$Si are presented in Fig. 4. The total DOS shows several interesting features which can be better understood by examining the partial DOS. The lowest peak at -9.5 eV

includes high degree of hybridization of Pt electronic states with Si 3s states, which confirms a covalent interaction between Pt and Si atoms. This peak is well separated by a gap of 1.3 eV from the main valence band region from -7.6 eV to 0 (the Fermi level). For energy window from -7.6 to -0.6 eV, the DOS features are mainly characterized by Pt1 and Pt2 5d orbitals with lesser contribution from La 5d and Si 3p orbitals. We have to identify the origin of the density of states at the Fermi level, which is crucial for governing superconducting properties since Cooper pairs are constituted by electrons which possess energies close to Fermi level. The partial DOS indicates that, although the contributions from the Pt atoms dominate near the Fermi level, all three atomic species are involved in the bands at and just above the Fermi level; note specially that La is not fully ionized to the 3^+ state. The characters at the Fermi level consist primarily as the Pt(1,2) 5d, La 5d, Si 3p and Pt(1,2) 6p states. This picture confirms that LaPt$_3$Si is a strongly three-dimensional metal with all atoms contributing to the metallic character. The value of the DOS at the Fermi level ($N(E_F)$) with SOI amounts to 2.57 States/eV, which is almost equal to the corresponding value of 2.59 States/eV without SOI. This result confirms our hypothesis that a mixing of spin-singlet and spin-triplet components in the superconducting condensate is weak and spin-singlet Cooper pairs dominate. The contributions of La, Pt1, Pt2, Si to $N(E_F)$ are approximately 23%, 41%, 23% and 13%. In particular, the total contribution of Pt1 and Pt2 atoms to $N(E_F)$ is approximately 64%. Thus, we can conclude that the d and p electrons of Pt(1,2) have the main effect on the superconducting properties of LaPt$_3$Si because a large density of states at the Fermi level ($N(E_F)$) gives rise to an enhancement in the electron-phonon coupling parameter (λ) according to the McMillan-Hopfield expression

$$\lambda = \frac{N(E_F) < I^2 >}{M < \omega^2 >}, \tag{1}$$

where $< \omega^2 >$ signals the average of squared phonon frequencies, M is the average atomic mass, and $< I^2 >$ is the Fermi surface average of squared electron-phonon coupling interaction. According to the McMillan-Hopfield expression, the value of electron-phonon coupling constant (λ) grows linearly with rising $N(E_F)$.

Fig. 5(a) shows the electronic band structure of LaPtSi$_3$ with and without SOI. As is the case with LaPt$_3$Si, when SOI is included, the degeneracy of the electronic bands is lifted along all basal-plane directions, but not along the Z-Γ symmetry direction. When SOI is included, fourfold and sixfold band-degeneracies are lifted in all crystal types, even in crystals with inversion symmetry. However, two-fold degeneracies would only be lifted perpendicular to directions along which the inversion symmetry is missing. In both materials considered in this work, inversion symmetry is not conserved along z-axis and thus two-fold degeneracies are not lifted along the Γ-Z and X-R directions. In Fig. 5(a), the bands close to the Fermi level are split by an amount of at most 50-200 meV. In order to analyse the electronic band structure of LaPtSi$_3$ in detail, its total and partial DOS are calculated and presented in Fig. 5 (b). We can see that the DOS features below -6.5 eV are mainly contributed by Si(1,2) electronic states with some contributions from the electronic states of La

and Pt electronic states. Thus, we can conclude that the bands in this region have a complex character. For the energy window from -6.5 to -3.0 eV, there is a high degree of hybridization of Pt d orbitals with Si(1,2) p orbitals, which highlights a covalent interaction in this material. The main valence band complex (from -3.0 eV to the Fermi level) consists of contributions from all atoms in the material. Furthermore, near the Fermi level, electronic bands show an appreciable dispersion along the Z-Γ symmetry direction, indicating that this material is also a three-dimensional metal in spite of the visible two dimensionality in its atomic structure. The orbital analysis of the DOS reveals the following atomic contributions: La (23%), Pt (20%), Si1 (18%) and Si2 (39%). The total DOS at the Fermi level ($N(E_F)$ without SOI is 1.51 States/eV, and with SOI is 1.50 States/eV. Once again, the effect of SOI on the value of $N(E_F)$ is negligible. We have to mention that a similar observation has been made for CaIrSi$_3$ [24] which is a compound isostructural to LaPtSi$_3$. Furthermore, we have to mention that the total contribution of Si(1,2) p states to $N(E_F)$ is around 50%. Thus, we suggest that the p electrons of Si atoms and Si-related vibrations play an important role in the determination of the superconducting critical temperature of LaPtSi$_3$.

2.2 Phonons and electron-phonon interaction

LaPt$_3$Si: We first examine the zone-centre phonon modes of LaPt$_3$Si classified by the irreducible representations of the simple tetragonal point group c$_{4v}$(4mm). The simple tetragonal structure of LaPt$_3$Si has twelve zone-centre optical phonon modes

$$\Gamma(c_{4v}(4mm)) = 3A_1 \; \oplus \; 4E \; \oplus \; B_1.$$

Phonon modes with one-dimensional representations A and B contain vibrations of relevant atoms along the z–direction, while modes with doubly-degenerate representation E atomic vibrations of relevant atoms in the x–y plane. The frequencies of the zone-centre phonon modes with and without SOI are given together with their electron-phonon coupling parameters in Tab. 2. This table clearly depicts that the influence of SOI on the zone-centre phonon frequencies and their electron-phonon coupling parameters is tiny. This result is expected because the effect of SOI for LaPt$_3$Si in a small energy window around the Fermi level is rather small. Further analysis of Tab. 2 shows that the electron-phonon coupling parameter for the lowest A_1 and B_1 modes is larger than the corresponding parameter for the rest of zone-centre phonon modes. Thus, it will be interesting to examine the atomic displacement patterns of these two phonon modes. These are presented in Fig. 6. The lowest A_1 mode arises from opposing vibrations of Pt and Si atoms against La atom along the z–axis while the B_1 mode involves only the same type Pt atoms oscillating against each other along the z–axis. We have to mention that both phonon modes include considerable vibrational contribution from Pt atoms. This result is expected because strong displacements of Pt atoms can give rise to strong electron-phonon interaction due to the significant contribution of Pt d electrons at the Fermi level.

Fig. 7 illustrates the phonon dispersion spectrum of LaPt$_3$Si along different symme-

try lines of the simple tetragonal. Brillouin zone and the corresponding total and atom-projected density of states. A few remarkable features of the phonon spectrum can be noted. Firstly, no imaginary phonon frequency modes are found at any symmetry direction. Thus, at the calculated equilibrium volume of $LaPt_3Si$, all phonon modes are stable, indicating $LaPt_3Si$ is stable dynamically in the simple tetragonal $CePt_3B$ structure. Secondly, there are two forbidden gaps with frequencies of magnitudes 4.1 and 2.3 THz in the phonon dispersion relations of $LaPt_3Si$ due to large mass difference between La (or Pt) and Si atoms. Thirdly, because of these two forbidden gaps, the phonon dispersion spectrum for $LaPt_3Si$ can be divided into three definite regions: first frequency band (FFB) (0-5.3 THz), second frequency band (SFB)(9.4-9.7 THz), and third frequency band (TFB) (12.0-12.80 THz). There are three acoustic and nine optical branches extending up to 5.3 THz in the FFB and the acoustic phonon modes are dispersive up to 2.8 THz. All nine optical phonon modes in this frequency region are also dispersive like the three acoustic phonon modes. However, both optical phonon modes in the SFB and the highest optical phonon mode in the TFB are nearly flat. The nature of the phonon dispersion relation can be well understood from the total and partial phonon density of states. Analyzing the total and atom-projected density of states in Fig. 7, one can see that, as expected, Si as the lightest element in the material dominates the SFB and TFB. However, a much smaller Si contribution has been observed in the FFB, while Pt, the heaviest atom, dominates this frequency band. Furthermore, La atom also makes significant contribution to the FFB due to its heavier mass than the mass of Si atom.

As we have mentioned before, Krannich and co-workers [20] have recently investigated the dispersion of transverse acoustic and low energy optical branches for $CePt_3Si$ along the Γ-M direction. Since $CePt_3Si$ is isostructural to $LaPt_3Si$ and the ionic radius and local environment of Ce and La are similar, the major difference in their phonon spectrum is expected to come from the mass difference between Ce and La. Thus, we have calculated the dispersion of phonon branches for $CePt_3Si$ along the Γ-M direction by using the force constant matrix of $LaPt_3Si$. Fig. 8 presents comparison of calculated (lines) and experimental data (filled squares). Our calculated results for $CePt_3Si$ are in good agreement with experimental data [20]. As we have mentioned before, the influence of SOI on phonons in $LaPt_3Si$ is very small. As a consequence, we can emphasize that the lattice dynamics of both materials are conventional. Furthermore, we can conclude that the ASOC plays less important role in these noncentrosymmetric superconductors than is commonly thought. We have to mention that a similar observation has been made in the LDA work of Krannich and co-workers [20].

LaPtSi$_3$: The primitive unit cell of body-centred tetragonal $LaPtSi_3$ includes one formula unit (total five atoms), giving a total of 15 phonon bands, containing three acoustic bands and twelve optical bands. The zone-centre optical phonon modes correspond to following irreducible representations:

$$\Gamma(c_{4v}(4mm)) = 4E \ \oplus 3A_1 \ \oplus B_1.$$

The frequencies of zone-centre phonon modes for $LaPtSi_3$ with and without SOI are given together with their electron-phonon coupling parameters in Tab. 3. This table

evidently reveals that the influence of SOI on the zone-centre phonon frequencies and their electron-phonon coupling parameter is not very large. Our electron-phonon interactions results for LaPtSi$_3$ suggest that the electron-phonon coupling parameters of the B$_1$ and the highest A$_1$ phonon modes are larger than the corresponding parameters for the rest of phonon modes. The eigenvector representations of these phonon modes are illustrated in Fig. 9. For the highest A$_1$ phonon mode, Si2 atoms vibrate against each other along the [001] direction while the B$_1$ phonon mode arises due to opposing motion of Si1 and Si2 atoms. In contrast to LaPt$_3$Si, the phonon modes in LaPtSi$_3$ with larger electron-phonon coupling parameters do not include vibrations of Pt atoms. We have expected this result for LaPtSi$_3$ because the p electrons of Si(1,2) atoms make large contribution to $N(E_F)$. A similar observation has been made for the electron-phonon interaction in CaIrSi$_3$ [24] which is isostructural to LaPtSi$_3$.

Fig. 10 illustrates the phonon dispersion spectrum of LaPtSi$_3$ along different symmetry lines of the body-centred tetragonal Brillouin zone and the corresponding total and atom-projected density of states. Again, all phonon modes have positive frequencies, strongly suggesting that the optimized LaPtSi$_3$ structure is also dynamically stable. The phonon spectrum of LaPtSi$_3$ has a frequency range of about 11.7 THz. In particular, the phonon spectrum depicts a set of 8 branches extending up to around 6.8 THz, separated by a gap of 0.2 THz from high-frequency branches that lie between 7.0THz and 11.7 THz. The partial phonon density of states show that Si-related phonon densities are quite dispersive, contributing to lattice vibrations over the whole range of phonon frequencies due to its smaller mass than the masses of La and Pt. Modes comprised of vibrations of all three atomic species are located below 3.9 THz. However, La and Pt vibrations almost disappear above 3.9 THz due to their heavier masses.

The main target of this work is to view the strength of the electron-phonon interaction in LaPt$_3$Si and LaPtSi$_3$ in order to explicitly understand the source of superconductivity in these NCS superconductors. We display the Eliashberg function $\alpha^2F(\omega)$ and the average electron-phonon coupling parameter together in Fig 11. In general, the phonon frequency variation of the Eliashberg function for both materials is similar to the variation of their phonon density of states. From the knowledge of $\alpha^2F(\omega)$, we are able to obtain the average electron-phonon coupling constant λ, which gives a good measure of the overall strength of the electron-phonon interaction; it is given by

$$\lambda = \int \lambda(\omega)\mathrm{d}\omega = 2 \int \frac{\alpha^2F(\omega)}{\omega}\mathrm{d}\omega. \tag{2}$$

The value of the average electron-phonon coupling parameter λ is found to be 0.470 and 0.488 for LaPt$_3$Si and LaPtSi$_3$,respectively, which suggests that the electron-phonon interaction in both materials is of weak strength. When SOI is not included, these values are changed to 0.466 and 0.487 for LaPt$_3$Si and LaPtSi$_3$, respectively. Now, we can conclude that the effect of SOI on the value of the average electron-phonon coupling parameter is negligible for both materials. This finding certainly

supports our hypothesis that spin-singlet Cooper pairs dominate in both materials.

The value of superconducting transition temperature T_c can be calculated from the Allan-Dynes modification of the McMillian formula [27]

$$T_c = \frac{\omega_{\ln}}{1.2}\exp\left(-\frac{1.04(1+\lambda)}{\lambda - \mu^*(1+0.62\lambda)}\right), \tag{3}$$

which links the value of T_c with λ, the logaritmically averaged phonon frequency $\omega_{\ln} = \exp\left(2\lambda^{-1}\int_0^\infty \frac{d\omega}{\omega}\alpha^2 F(\omega)\ln\omega\right)$, and the effective screened Coulomb repulsion constant μ^*. The value of μ^* is taken to be 0.13 for both materials while the value of $\omega_{\ln}$ is determined to be 126.61 K and 213.94 K for LaPt$_3$Si and LaPtSi$_3$, respectively. Inserting the values of λ, $\omega_{\ln}$ and μ^* in Eq. (3), the value of T_c is obtained to be 0.67 K and 1.39 K for LaPt$_3$Si and LaPtSi$_3$, respectively. These values compare very well with the respective experimental values of 0.65 K [1] and 1.52 K [19]. We thus conclude that in spite of their layered structures, in LaPt$_3$Si and LaPtSi$_3$ superconductivity can be explained in terms of conventional weak-coupling theory, a situation similar to CaIrSi$_3$ [24].

The electronic specific heat coefficient (γ) is related to $N(E_F)$ and λ by

$$\gamma = \frac{1}{3}\pi^2 k_B^2 N(E_F)(1+\lambda). \tag{4}$$

Using the above equation, the value of γ is calculated to be 8.9 $\frac{mJ}{molK^2}$ and 5.2 $\frac{mJ}{molK^2}$ for LaPt$_3$Si and LaPtSi$_3$, respectively. The calculated value of γ for LaPt$_3$Si is in excellent accordance with its experimental value of of 9 $\frac{mJ}{molK^2}$ [1], while the calculated value of γ for LaPtSi$_3$ deviates from its experimental value of 4.4 $\frac{mJ}{molK^2}$ [19] within 20%. We think that this descrepancy arises as a result of joint error margins in the experimental and theoretical estimates. For example, the value of γ for superconductor BaPt$_4$Ge$_{12}$ is estimated to be 42 and 34 $\frac{mJ}{molK^2}$, respectively, by different experimental groups [33,34]. The difference between these values is more than %20. Thus, we can conclude that the calculated value of γ for LaPtSi$_3$ is in accaptable agreement with its experimental value of 4.4 $\frac{mJ}{molK^2}$ [19]. The observed agreement supports that the scenario for superconductivity in these noncentrosymmetric superconductors is conventional rather than an exotic one.

Finally, it will be interesting to compare our results for LaPt$_3$Si with previous results for NdPt$_3$Si [35,36]. These materials are isostructural to each other. However, NdPt$_3$Si [36] displays magnetic order rather that superconducting state. The value of N(E$_F$) for NdPt$_3$Si is found to 3.2 States/eV which is larger that the corresponding value of 2.57 States/eV for LaPt$_3$Si. However, the value of γ for NdPt$_3$Si [36] is found to be 7.54 $\frac{mJ}{molK^2}$ which is lower that the corresponding value of 8.94 $\frac{mJ}{molK^2}$. From Eq. 4, the value of λ for NdPt$_3$Si is obtained almost zero. This finding explains why NdPt$_3$Si does not show superconductivity, while its isostructural LaPt$_3$Si is superconductor.

3   Summary

In this study, we have presented a detailed *ab initio* analysis of the structural, electronic, phononic and superconducting properties of LaPt$_3$Si and LaPtSi$_3$ with and without SOI by using the generalised gradient approximation of the density functional theory and the linear response approach. Our structural results for both noncentrosymmetric (NCS) superconductors agree well with available experimental results. In particular, the value of bulk modulus is found to be 145.6 GPa for LaPt$_3$Si and 117.1 GPa for LaPtSi$_3$. Unfortunately, there are no previous experimental and theoretical results for the bulk modulus for both materials and thus we expect that our theoretical calculations will encourage future experimental and theoretical studies. Our electronic calculations reveal that both materials are strongly three dimensional with all atoms contributing to their metallic character in spite of the apparent two dimensionality in their electronic structures. From a critical assessment of the total and partial electronic states, we have observed that the states close to the Fermi level are primary contributed by Pt electronic states for LaPt$_3$Si and Si electronic states for LaPtSi$_3$. This result asserts active roles of Pt and Si atoms in obtaining the electronic and superconducting properties of LaPt$_3$Si and LaPtSi$_3$, respectively. Our phonon calculations reveal that all phonon modes for both materials have real positive frequencies, strongly indicating that the optimized LaPt$_3$Si and LaPtSi$_3$ structures are dynamical stable.

Our electron-phonon interaction results for these NCS superconductors show that the effect of SOI interaction on the Eliashberg function $\alpha^2 F(\omega)$ and the average electron-phonon coupling parameter λ is very small. This result confirms that a mixing of the spin-singlet and the spin-triplet components in these superconductors is weak and that the spin-singlet Cooper pairs dominate. Thus, we conclude that superconductivity in these noncentrosymmetric superconductors has conventional origin rather than an exotic one. By integrating the Eliashberg spectral function, the average electron-phonon coupling parameter λ is obtained to be 0.470 for LaPt$_3$Si and 0.488 for LaPtSi$_3$, suggesting that these materials are weak-coupling BCS superconductors. Using the Allen-Dynes modified McMillian equation, with the screened Coulomb pseudopotential parameter $\mu^* = 0.13$, the superconducting temperature is calculated to be 0.67 K for LaPt$_3$Si and 1.39 K for LaPtSi$_3$. These values are in good accordance with their experimental values of 0.65 K for LaPt$_3$Si and 1.52 K for LaPtSi$_3$.

References

[1] E. Bauer, G. Hilscher, H. Michor, Ch. Paul, E. W. Scheidt, A. Gribanov, Yu. Seropegin, H. Noël, M. Sigrist, P. Rogl,Heavy Fermion Superconductivity and Magnetic Order in Noncentrosymmetric $CePt_3Si$, Phys. Rev. Lett. 92 (2004) 027003.

[2] V. M. Edelstein,Characteristics of the Cooper pairing in two-dimensional noncentrosymmetric electron systems, Sov. Phys. JETP 68 (1989) 1244-1249.

[3] L. P. Gorkov, E. I. Rashba, Superconducting 2D System with Lifted Spin Degeneracy: Mixed Singlet-Triplet State, Phys. Rev. Lett. 87 (2001) 037004.

[4] V. M. Edelstein, Magnetoelectric Effect in Polar Superconductors, Phys. Rev. Lett. 75 (1995) 2004-2007.

[5] P. A. Frigeri, D. F. Agterberg, A. Koga, M. Sigrist, Superconductivity without Inversion Symmetry: MnSi versus $CePt_3Si$, Phys. Rev. Lett. 92 (2004) 097001.

[6] E. Bauer, M. Sigrist, Non-Centrosymmetric Superconductors: Introduction and Overview (Springer, Berlin, 2012), Vol. 847.

[7] T. Akazawa, H. Hidaka, T. Fujiwara, T. Kobayashi, E. Yamamoto, Y. Haga, R. Settai, Y. Onuki,Pressure-induced superconductivity in ferromagnetic UIr without inversion symmetry, J. Phys.: Condens. Matter 16 (2004) L29-L32.

[8] H. Q. Yuan, D. F. Agterberg, N. Hayashi, P. Badica, D. Vandervelde, K. Togano, M. Sigrist, M. B. Salamon, S-Wave Spin-Triplet Order in Superconductors without Inversion Symmetry: Li_2Pd_3B and Li_2Pt_3B, Phys. Rev. Lett. 97 (2006) 017006.

[9] J. Chen, M. B. Salamon, S. Akutagawa, J. Akimitsu, J. Singleton, J. L. Zhang, L. Jiao, H. Q. Yuan,Evidence of nodal gap structure in the noncentrosymmetric superconductor Y_2C_3, Phys. Rev. B 83 (2011) 144529.

[10] S. Hashimoto, T. Yasuda, T. Kubo, H. Shishido, T. Ueda, R. Settai, T. D Matsuda, Y. Haga, H. Harima, Y. Õnuki, The de Haasvan Alphen effect and the Fermi surface in $CePt_3Si$ and $LaPt_3Si$, J. Phys.: Condens. Matter 16 (2004) L287–L296

[11] M. Yogi, Y. Kitaoka, S. Hashimoto, T. Yasuda, R. Settai, T.D. Matsuda, Y. Haga, Y. Õnuki, P. Rogl, E. Bauer, ^{195}Pt NMR study on noncentrosymmetric heavy-fermion superconductor $CePt_3Si$, J. Phys. Chem. Solids 67 (2006) 522-524.

[12] T. Takeuchi, T. Yasuda, M. Tsujino, H. Shishido, R. Settai, H. Harima, Y. Õnuki, Specific Heat and de Haasvan Alphen Experiments on the Heavy-Fermion Superconductor $CePt_3Si$, J. Phys. Soc. Jpn. 76 (2007) 014702.

[13] R. L. Ribeiro, I. Bonalde, Y. Haga, R. Settai, Y. Õnuki, Magnetic Penetration Depth and Gap Symmetry of the Noncentrosymmetric Superconductors $CePt_3Si$ and $LaPt_3Si$, J. Phys. Soc. Jpn. 78 (2009) 115002.

[14] M. Shiotsuki, G. Motoyama, Y. Oda, A. Yamaguchi, A. Sumiyama, T. Takeuchi, R. Settai, Y. Õnuki, Specific Heat on the Non-centrosymmetric Superconductor $LaPt_3Si$, J. Phys. Soc. Jpn. 80 (2011) SA070.

[15] E. Bauer, R. T. Khan, H. Michor, E. Royanian, A. Grytsiv, N. Melnychenko-Koblyuk, P. Rogl, D. Reith, R. Podloucky, E.-W. Scheidt, W. Wolf, M. Marsman , BaPtSi$_3$: A noncentrosymmetric BCS-like superconductor, Phys. Rev. B 80 (2009) 064504.

[16] V.K. Anand, A. D. Hillier, D. T. Adroja, A. M. Strydom, H. Michor, K. A. McEwen, B. D. Rainford, Specific heat and SR study on the noncentrosymmetric superconductor LaRhSi$_3$, Phys. Rev. B 83 (2011) 064522.

[17] G. Eguchi, D. C. Peets, M. Kriener, Y. Maeno, E. Nishibori, Y. Kumazawa, K. Banno, S. Maki, H. Sawa, Crystallographic and superconducting properties of the fully gapped noncentrosymmetric 5d-electron superconductors CaMSi$_3$ (M= Ir, Pt), Phys. Rev. B 83 (2011) 024512.

[18] R.P. Singh, A. D. Hillier, D. Chowdhury, J. A. T. Barker, D. McK. Paul, M. R. Lees, G. Balakrishnan, Probing the superconducting ground state of the noncentrosymmetric superconductors CaTSi$_3$ (T = Ir, Pt) using muon-spin relaxation and rotation, Phys. Rev. B 90 (2014) 104504.

[19] M. Smidman, A. D. Hillier, D. T. Adroja, M.R. Lees, V. K. Anand, R. P. Singh, R. I. Smith, D. M. Paul, G. Balakrishnan, Investigations of the superconducting states of noncentrosymmetric LaPdSi$_3$ and LaPtSi$_3$, Phys. Rev.B 89 (2014) 094509.

[20] S. Krannich, D. Lamago, D. Manske, E. Bauer, A. Prokofiev, R. Heid, K.-P. Bohnen, F. Weber, Absence of spin-orbit coupling induced effects on the lattice dynamics in CePt$_3$Si, Phys. Rev.B 92 (2015) 125137.

[21] V.V. Bannikov, I.R. Shein , A.L. Ivanovskii,Structural and Electronic Properties and the Fermi Surface of the New Noncentrosymmetric Superconductors: 3.6 K CaIrSi$_3$ and 2.3 K CaPtSi$_3$, JETP Lett. 92 (2010) 343-347.

[22] T. Terashima, M. Kimata, S. Uji, T. Sugawara, N. Kimura, H. Aoki, H. Harima, Fermi surface in LaRhSi$_3$ and CeRhSi$_3$, Phys. Rev.B 78 (2008) 205107.

[23] M.J. Winiarski, M. Samsel-Czekala, Electronic structure of non-centrosymmetric superconductor LaPdSi$_3$ and its reference compound LaPdGe$_3$, Intermetallics, 56 (2015) 44-47.

[24] H.Y. Uzunok, E. İpsara, H.M. Tütüncü, G.P. Srivastava, A. Başoğlu, The effect of spin orbit interaction for superconductivity in the noncentrosymmetric superconductor CaIrSi$_3$, J. Alloys Compd. 681 (2016) 205-211.

[25] P. Giannozzi, S. Baroni, N. Bonini, M. Calandra, R. Car, C. Cavazzoni, D. Ceresoli, G. L. Chiarotti, M. Cococcioni, I. Dabo, A.D. Corso, S. de Gironcoli, S. Fabris, G. Fratesi, R. Gebauer, U. Gerstmann, C. Gougoussis, A. Kokalj, M. Lazzeri, L. Martin-Samos, N. Marzari, F. Mauri, R. Mazzarello, S. Paolini, A. Pasquarello, L. Paulatto, C. Sbraccia, S. Scandolo, G. Sclauzero, A.P. Seitsonen, A. Smogunov, P. Umari, R.M. Wentzcovitch, QUANTUM ESPRESSO: a modular and open-source software project for quantum simulations of materials J. Phys.: Condens. Matter 21 (2009) 395502.

[26] P. B. Allen, Neutron Spectroscopy of Superconductors, Phys. Rev. B 6 (1972) 2577.

[27] P. B. Allen, R. C. Dynes, Transition temperature of strong-coupled superconductors reanalyzed, Phys. Rev. B 12 (1975) 905.

[28] J. P. Perdew, K. Burke, M. Ernzerhof, Generalized Gradient Approximation Made Simple, Phys. Rev. Lett. 77 (1996) 3865.

[29] W. Kohn, L. J. Sham, Self-Consistent Equations Including Exchange and Correlation Effects, Phys. Rev. 140 (1965) A1133.

[30] H. J. Monkhorst, J. D. Pack, Special points for Brillouin-zone integrations, Phys. Rev. B 13 (1976) 5188-5192.

[31] F. D. Murnaghan, The Compressibility of Media under Extreme Pressures, Proc. Nat. Acad. Sci. USA 50 (1944) 697.

[32] H. M. Tütüncü, H. Y. Uzunok, Ertuğrul Karaca, G. P. Srivastava, S. Özer, Ş. Uğur, Ab initio investigation of BCS-type superconductivity in $LuNi_2B_2C$-type superconductors, Phys. Rev. B 92 (2015) 054510.

[33] E. Bauer, A. Grytsiv, Xing-Qiu Chen, N. Melnychenko-Koblyuk, G. Hilscher, H. Kaldarar, H. Michor, E. Royanian, G. Giester, M. Rotter, R. Podloucky, P. Rogl, Superconductivity in Novel Ge-Based Skutterudites: $Sr,BaPt_4Ge_{12}$, Phys. Rev. Lett. 99 (2007) 217001.

[34] R. Gumeniuk, W. Schnelle, H. Rosner, M. Nicklas, A. Leithe-Jasper, and Yu. Grin, Superconductivity in the Platinum Germanides MPt_4Ge_{12} (M=RareEarth or Alkaline-Earth Metal) with Filled Skutterudite Structure, Phys. Rev. Lett. 100 (2008) 017002.

[35] E. Bauer, R. Lackner, G. Hilscher, H. Michor, M. Sieberer, A. Eichler, A. Gribanov, Y. Seropegin, P. Rogl, $REPt_3Si$ (RE = La, Pr, Nd, Sm and Gd): isotypes of the heavy fermion superconductor $CePt_3Si$, J. Phys.:Conden. Matter 17 (2005) 1877.

[36] M. Diviŝ, J. Peltierová-Vejpravová, J. Rusz, H. Michor, G. Hilscher, P. Blaha, K. Schwarz, The electronic structure and crystal field of RPt_3Si (R=Pr, Nd, Sm), Phys. B Condens. Matter 400 (2007) 114-118.
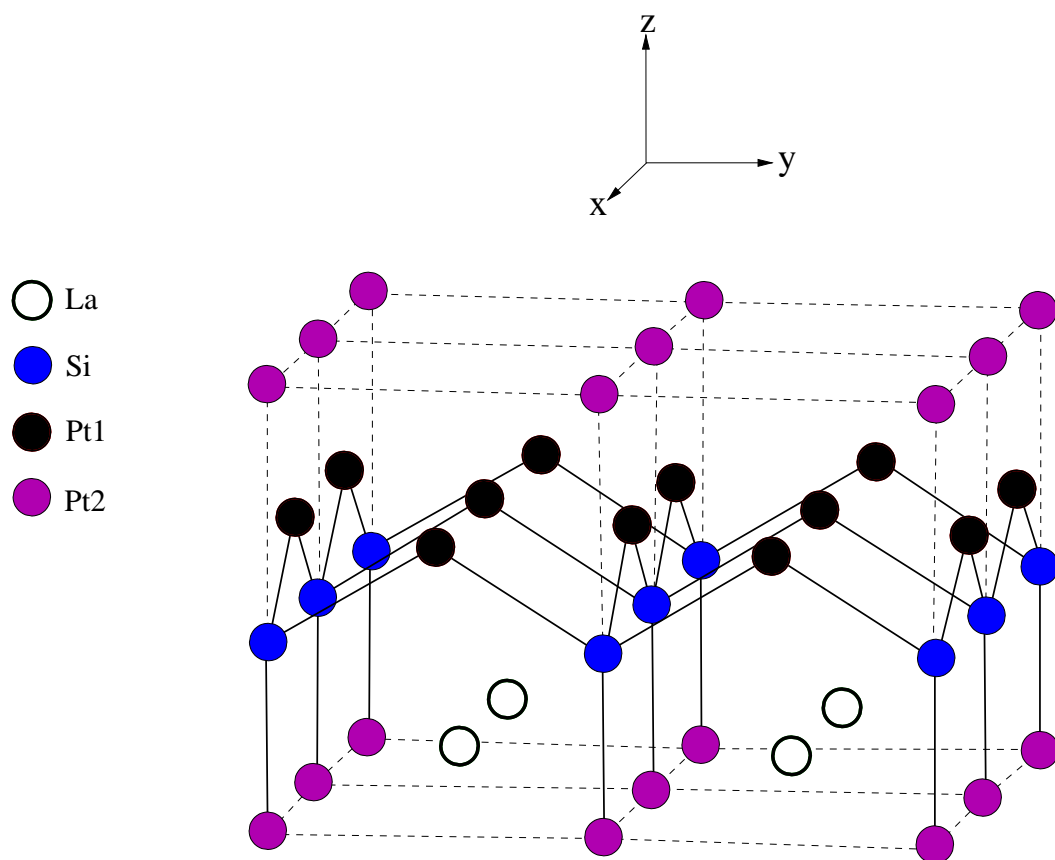
Fig. 1. The simple tetragonal structure of LaPt$_3$Si.
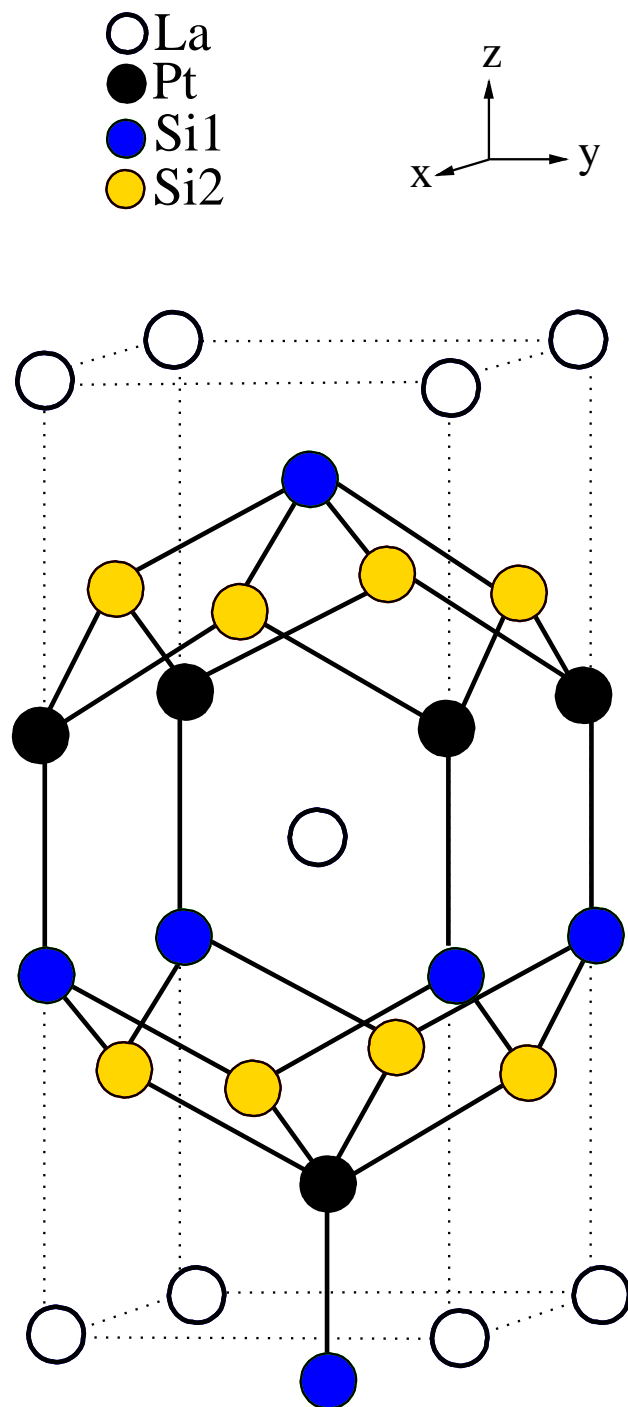
Fig. 2. The BaNiSn₃-type crystal structure of LaPtSi₃. The crystal structure has no mirror plane perpendicular to the z–axis.
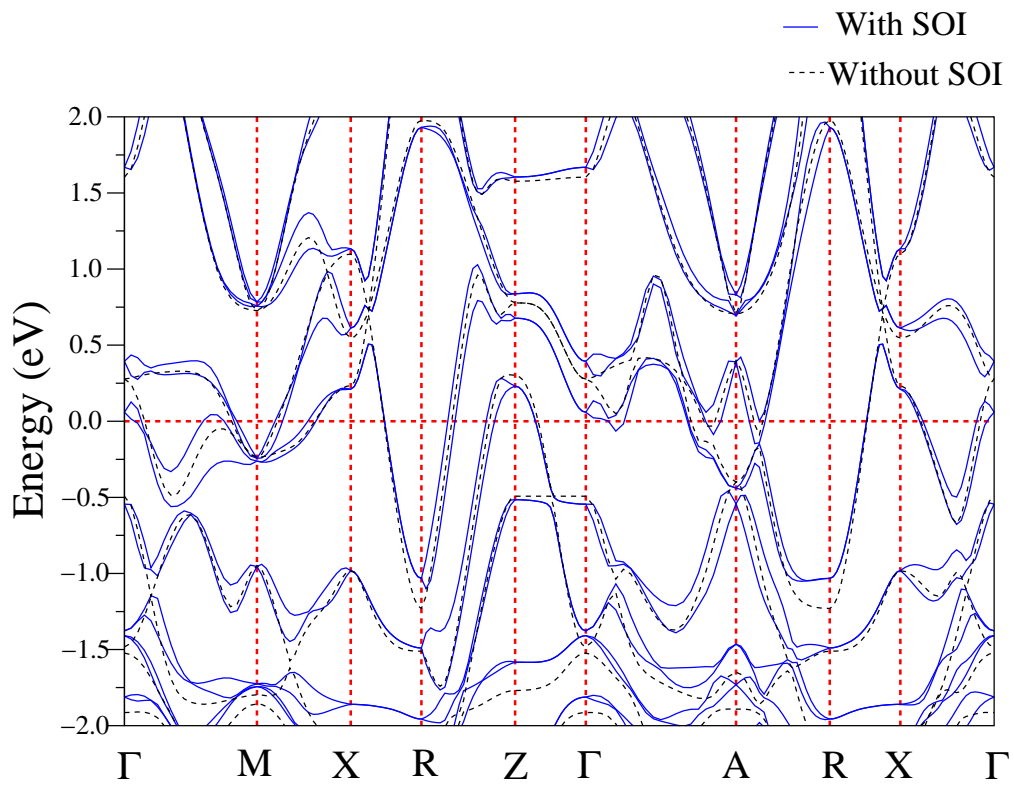
Fig. 3. Electronic band structure of LaPt₃Si for high symmetry lines of the simple tetragonal crystal structure with and without SOI.
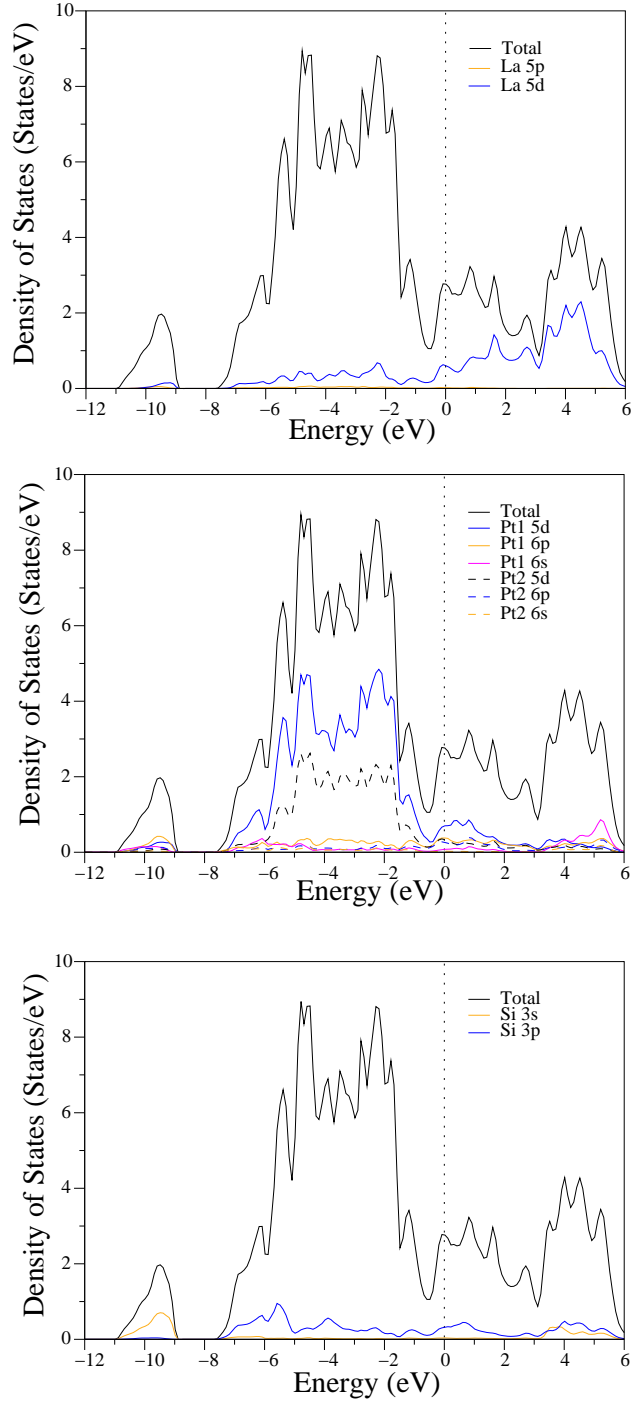
Fig. 4. The calculated total and partial electronic density of states (DOS) with SOI for LaPt$_3$Si. The dashed line represents the Fermi energy level, E_F.

18

(a)

(b)
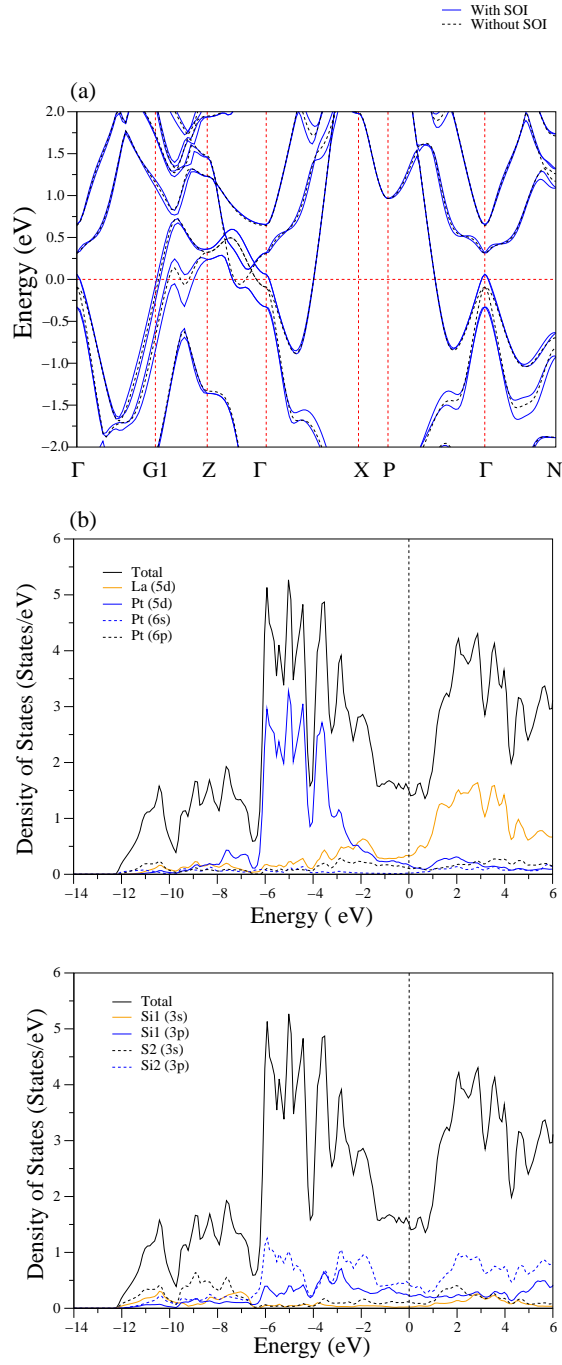
Fig. 5. (a) Electronic band structure of LaPtSi$_3$ for high symmetry lines of the body-centred tetragonal crystal structure with and without SOI. (b) The calculated total and partial density of states (DOS) with SOI for LaPtSi$_3$. The dashed line represents the Fermi energy level, E_F.

19
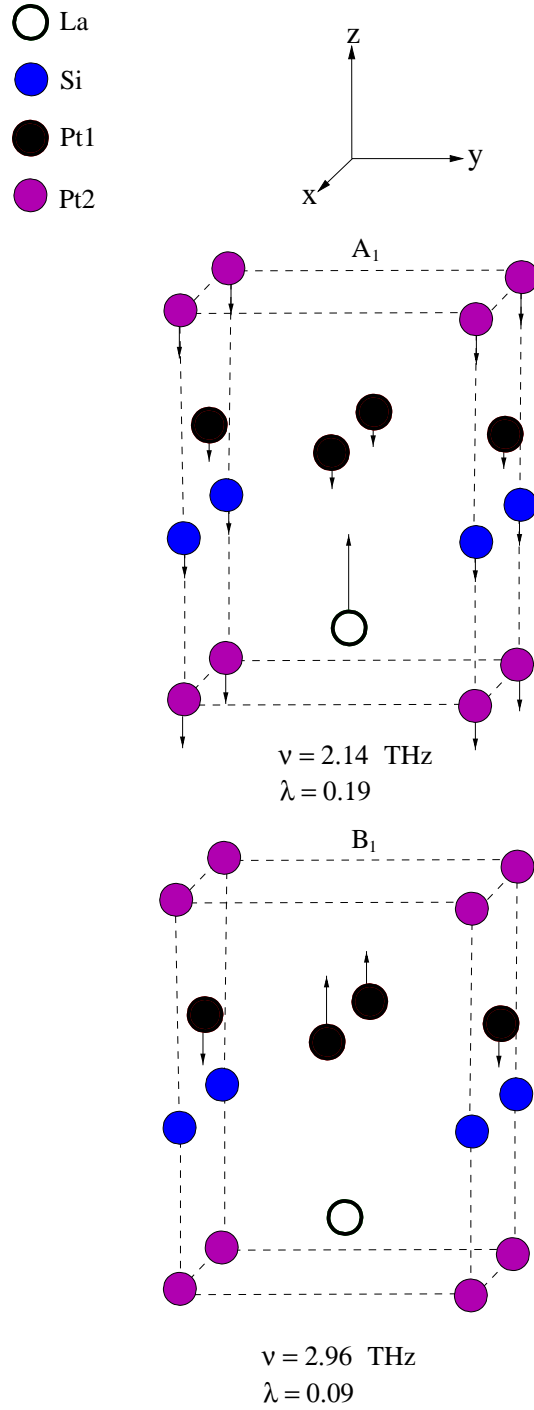
Fig. 6. Eigenvector representation of the lowest A_1 mode and the B_1 mode in $LaPt_3Si$.
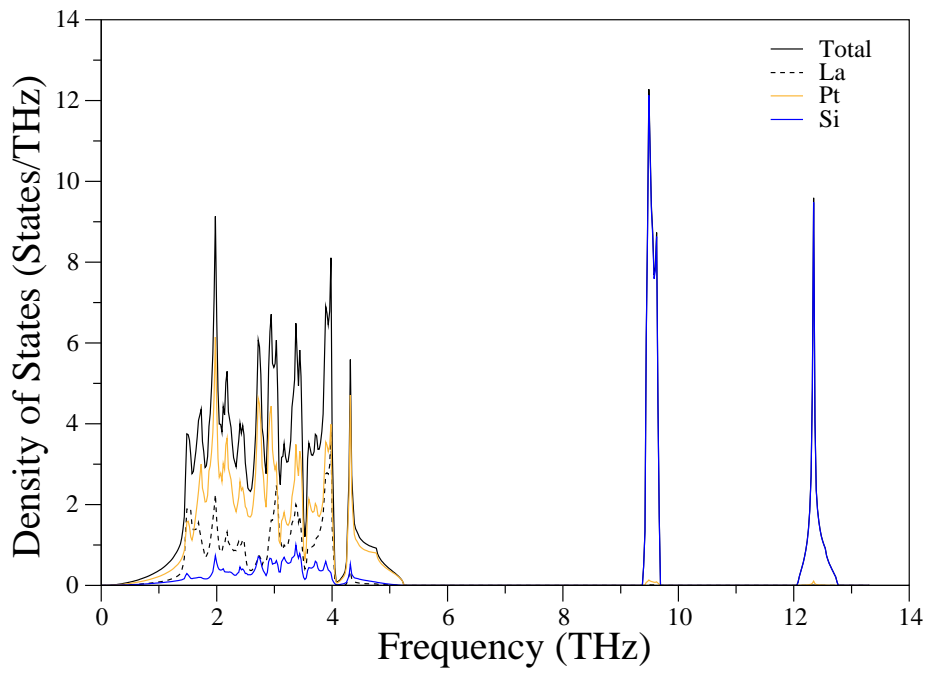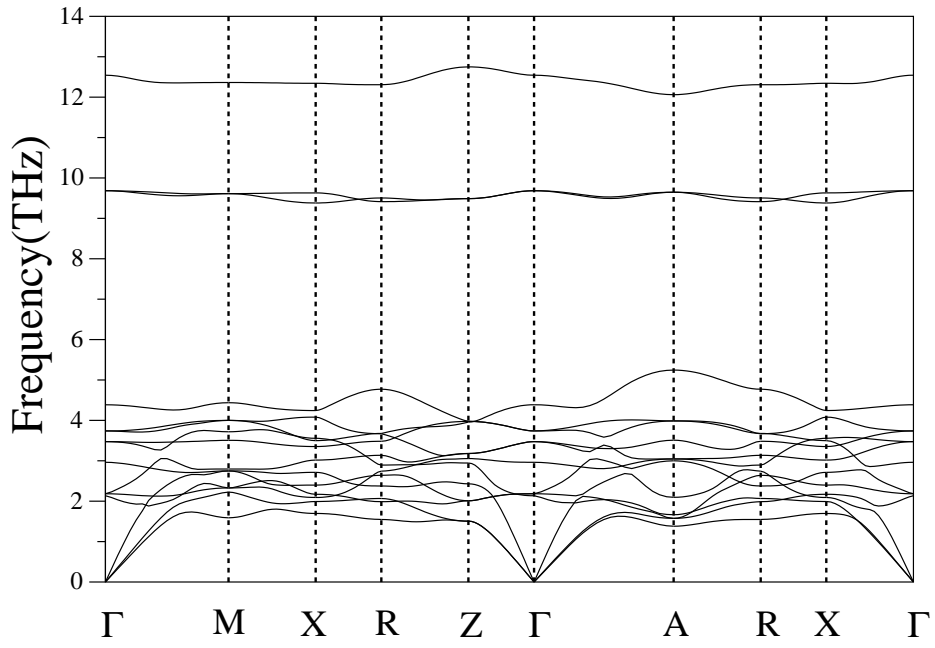
Fig. 7. The calculated phonon spectrum for LaPt$_3$Si and the corresponding total and atom-projected density of states.
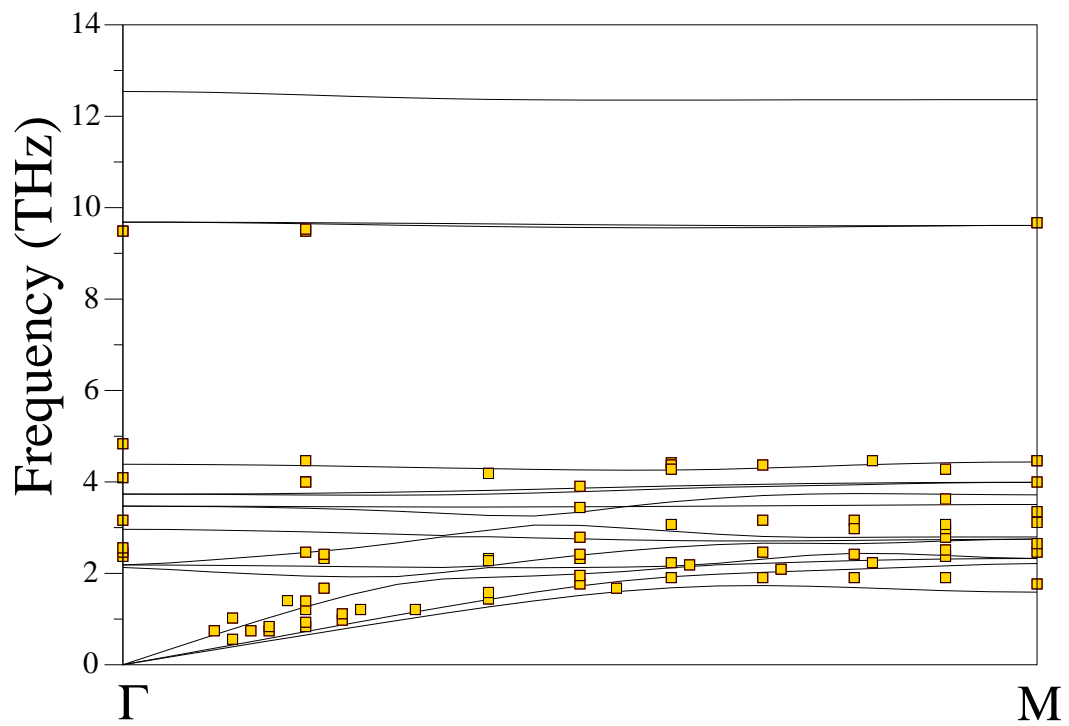
Fig. 8. The calculated phonon branches of CePt$_3$Si along the $\Gamma - M$ symmetry direction. The force constants for LaPt$_3$Si were used. The red squares show the experimental results from the inelastic neutron scattering work of Krannich and co-workers [20].

La
Pt
Si1
Si2

z
x
y

B_1

A_1

$\nu = 8.35$ THz

$\lambda = 0.11$

$\nu = 11.21$ THz

$\lambda = 0.11$
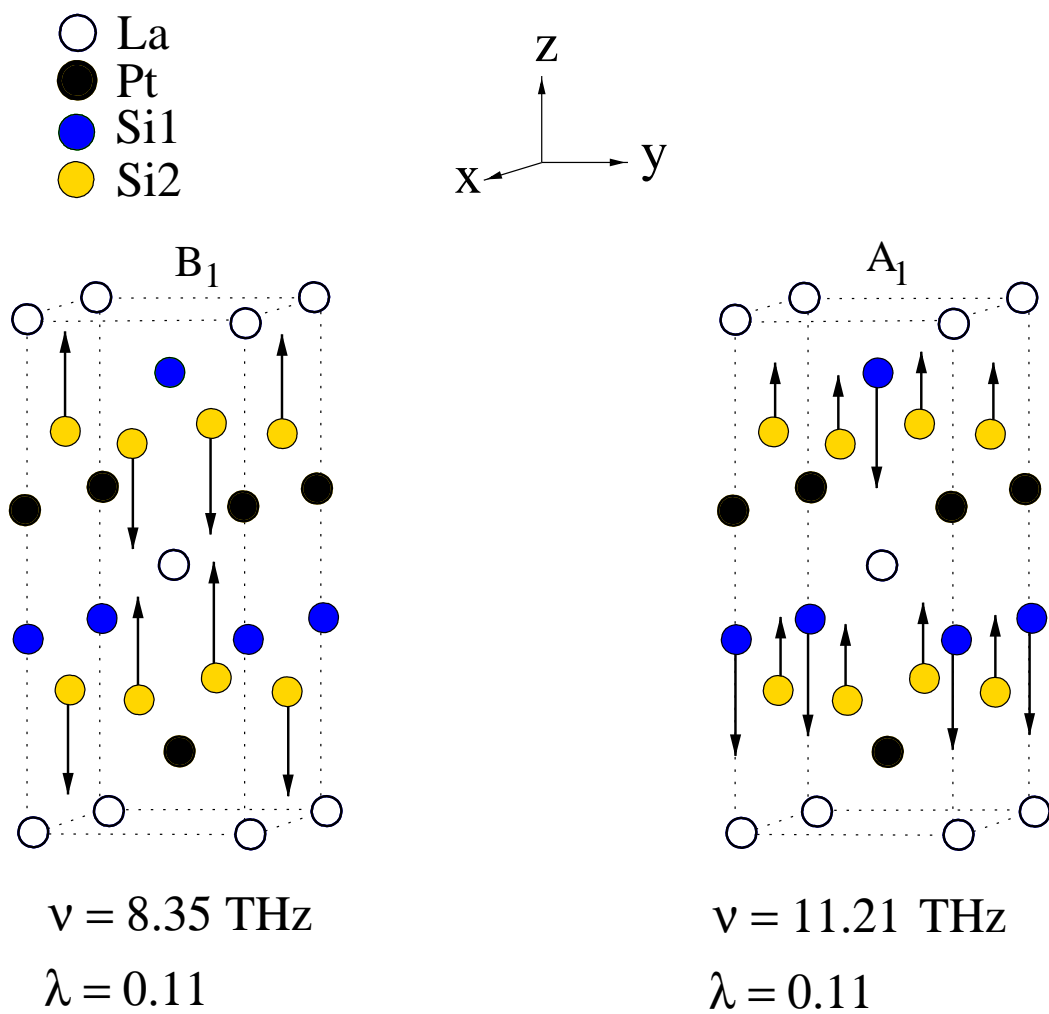
Fig. 9. Eigenvector representation of the B_1 mode and the highest A_1 mode in LaPtSi$_3$.
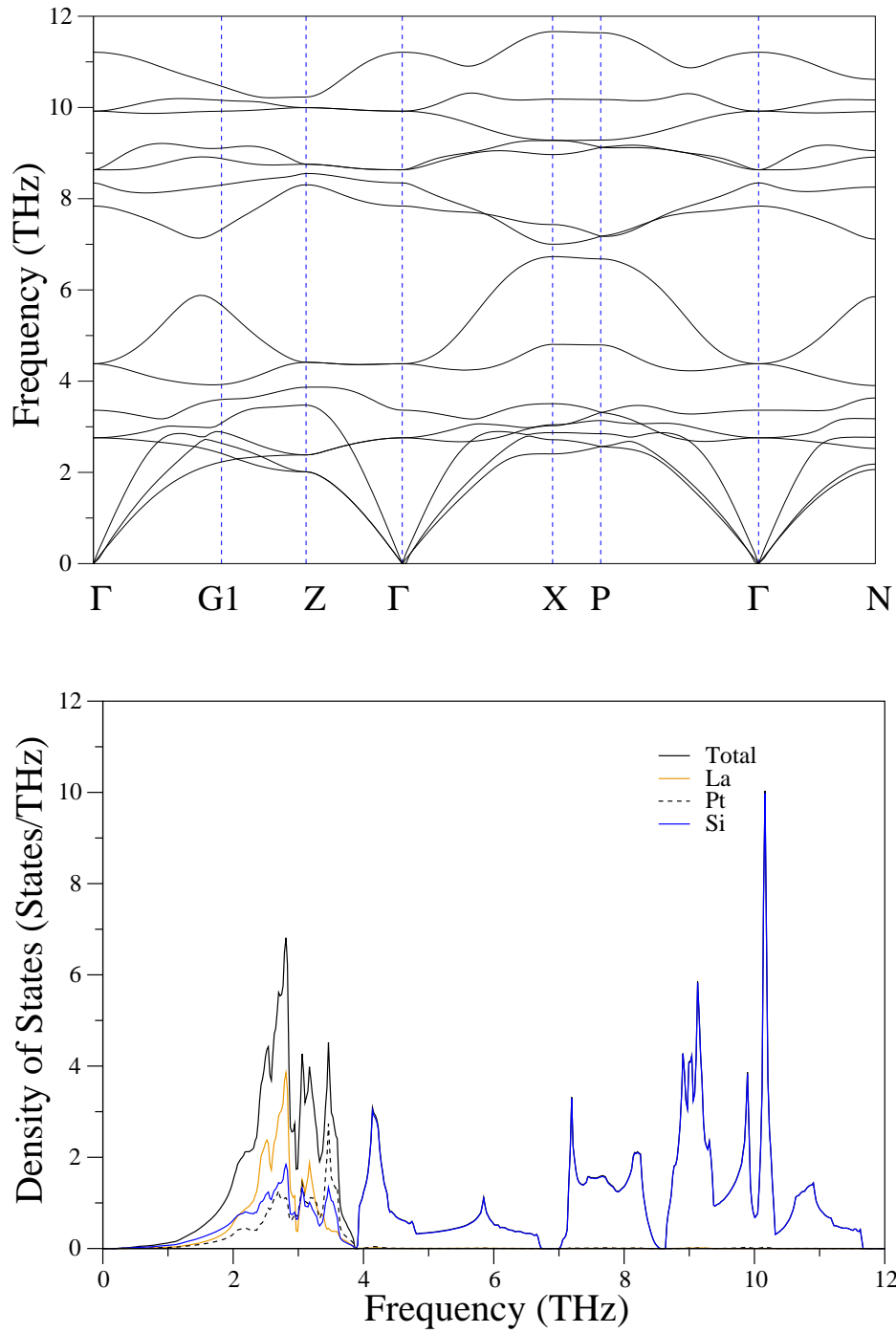
Fig. 10. The calculated phonon spectrum for LaPtSi₃ and the corresponding total and atom-projected density of states.
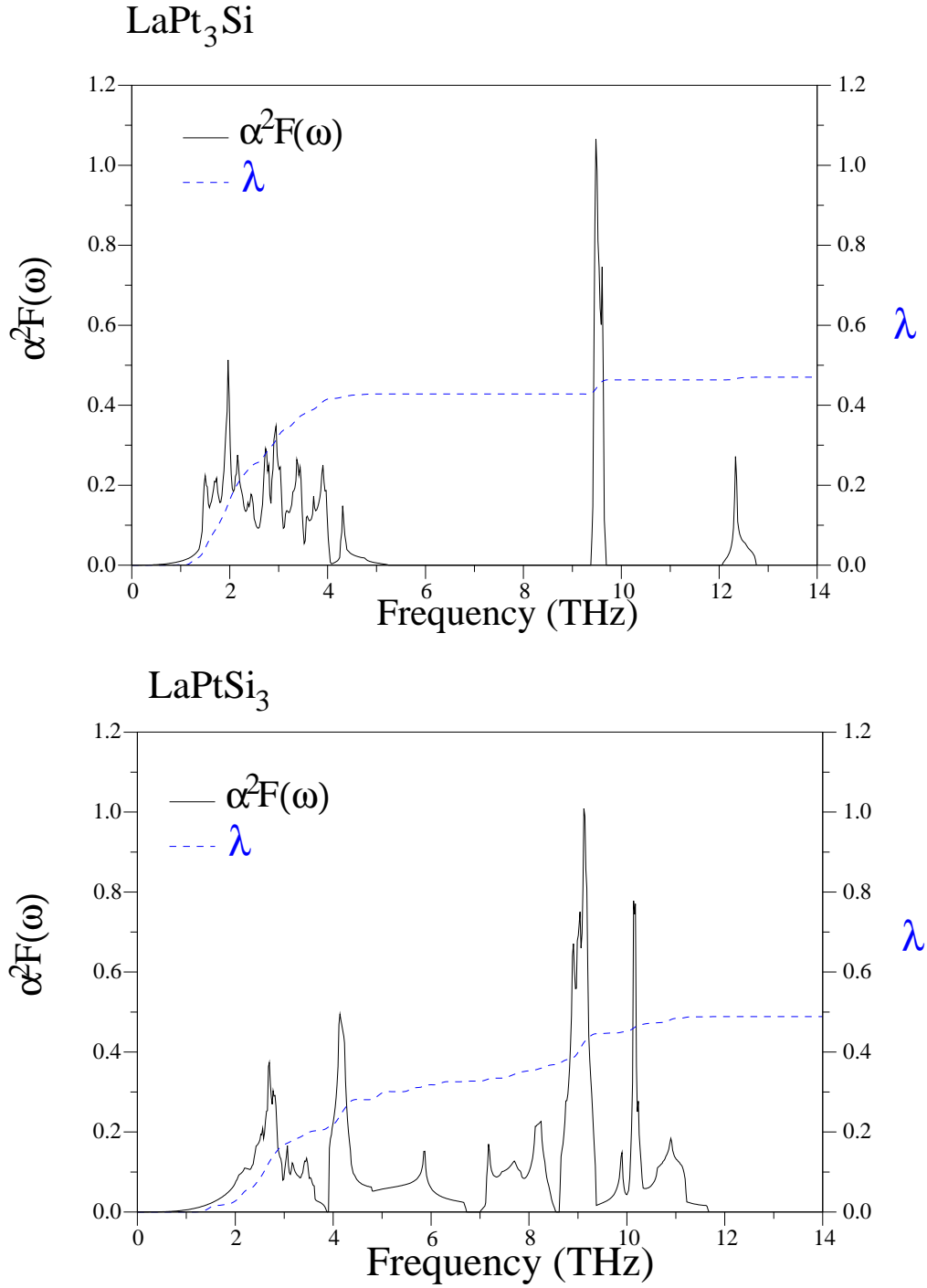
LaPt$_3$Si

LaPtSi$_3$

Fig. 11. The electron-phonon spectral function $\alpha^2F(\omega)$ (red line) and the average electron-phonon coupling parameter λ (blue line) for LaPt$_3$Si and LaPtSi$_3$.

Table 1

Structural parameters for LaPt$_3$Si (simple tetragonal) and LaPtSi$_3$ (body-centred tetragonal) their comparison with available experimental and theoretical results.

Material	$a(\mathring{A})$	$c(\mathring{A})$	$V(\mathring{A}^3)$	z_{La}	z_{Pt1}	z_{Si}	$d_{Pt1-Si}(\mathring{A})$	$d_{Pt2-Si}(\mathring{A})$	B(GPa)
LaPt$_3$Si	4.157	5.516	95.32	0.149	0.648	0.422	2.424	2.326	145.6
LDA [20]	4.072	5.442	90.23	0.147	0.650	0.412	2.424	2.242	
Experimental [1]	4.115	5.438	92.10						
Material	$a(\mathring{A})$	$c(\mathring{A})$	$V(\mathring{A}^3)$	z_{Pt}	z_{Si1}	z_{Si2}	$d_{Pt-Si1}(\mathring{A})$	$d_{Pt-Si2}(\mathring{A})$	B(GPa)
LaPtSi$_3$	4.376	9.672	95.63	0.647	0.395	0.261	2.441	2.360	117.1
Experimental [19]	4.347	9.637	91.07						

Table 2

Calculated zone-centre phonon frequencies (ν in THz) and their electron-phonon coupling parameters (λ) with and without spin-orbit interaction (SOI) for LaPt$_3$Si.

Mode	A$_1$	E	B$_1$	E	E	A$_1$	E	A$_1$
ν with SOI	2.14	2.18	2.96	3.47	3.74	4.39	9.68	12.54
ν without SOI	2.15	2.21	2.94	3.53	3.77	4.38	9.64	12.54
λ with SOI	0.19	0.03	0.09	0.03	0.03	0.02	0.01	0.01
λ without SOI	0.22	0.02	0.11	0.04	0.02	0.02	0.01	0.01

Table 3

Calculated zone-centre phonon frequencies (ν in THz) and their electron-phonon coupling parameters (λ) with and without spin-orbit interaction (SOI) for LaPtSi$_3$.

Mode	E	A$_1$	E	A$_1$	B$_1$	E	E	A$_1$
ν with SOI	2.76	3.36	4.38	7.84	8.34	8.63	9.92	11.21
ν without SOI	2.89	3.46	4.39	7.84	8.36	8.61	9.92	11.18
λ with SOI	0.08	0.07	0.06	0.03	0.11	0.05	0.02	0.11
λ without SOI	0.06	0.07	0.06	0.03	0.11	0.05	0.02	0.11